Physical properties of shallow ice cores from Antarctic and sub-Antarctic islands

Elizabeth Ruth Thomas[1], Guisella Gacitúa[2], Joel B.Pedro[3,4], Amy Constance Faith King[1],
5Bradley Markle[5], Mariusz Potocki[6,7], Dorothea Elisabeth Moser[1,8]

[1]British Antarctic Survey, Cambridge, CB3 0ET, UK

[2]Centro de Investigación Gaia Antártica, Universidad de Magallanes, Punta Arenas, Chile

[3]Australian Antarctic Division, Kingston, 7050, Australia

10[4]Australian Antarctic Programme Partnership, Hobart, Tasmania 7001 Australia

[5]California Institute of Technology, Pasadena, CA, USA, 91125

[6]Climate Change Institute, University of Maine, Orono, ME 04469, USA

[7]School of Earth and Climate Sciences, University of Maine, Orono, ME 04469, USA

[8]Institut für Geologie und Paläontologie, University of Münster, 48149 Münster, Germany

15

Abstract.

The sub-Antarctic is one of the most data sparse regions on earth. A number of glaciated Antarctic and sub-Antarctic islands have the potential to provide unique ice core records of past climate, atmospheric circulation and sea ice. However, very little is known about the glaciology of these remote islands or their vulnerability to
20warming atmospheric temperature. Here we present melt histories and density profiles from shallow ice (firn) cores (14 to 24 m) drilled on three sub-Antarctic islands and two Antarctic coastal domes. Additionally, complementary ground-penetrating radar (GPR) data were collected to further characterise each site and assess the spatial distribution of the observed melt layers. This study includes the first ever firn cores from Bouvet Island (54°26'0 S, 3°25'0 E) in the South Atlantic, from Peter 1st Island (68°50'0 S, 90°35'0 W) in the
25Bellingshausen Sea and from Young Island (66°17′S, 162°25′E) in the Ross Sea sector's Balleny Islands chain. Despite their sub-Antarctic location, surface melt is low at most sites (melt layers account for ~10% of total core), with undisturbed ice layers in the upper ~40 m, suggesting minimal impact of melt water percolation. The exception is Young Island, where melt layers account for 47% of the firn core. Surface snow densities range from 0.47 to 0.52 kg m^{-3}, with close-off depths ranging from 21 to 51 m. Based on the measured density, we
30estimate that the bottom ages of a 100 m ice core drilled on Peter 1st Island would reach ~1856 AD and ~1874 AD at Young Island.

1 Introduction

The sub-Antarctic region sits at the interface of polar and mid-latitude climate regimes, making it highly
35sensitive to shifting climate over time. However, the sub-Antarctic and the Southern Ocean is one of the most data sparse regions on earth. A recent compilation of climate data spanning the 20th century revealed that of the 692 records that exist globally (Emile-Geay et al., 2017), none are available for the Southern Ocean. The vast expanse of open water makes climate and paleoclimate observations difficult, but a number of glaciated sub-

1

Antarctic island (SAIs- defined here as islands south of the Southern Ocean polar front) may be suitable for 40 extracting paleoclimate information from ice cores (Figure 1).

Many of these SAIs sit within the westerly wind belt and the transitional sea-ice zone (Figure 1). Westerly winds drive ocean upwelling and basal melt of Antarctic ice shelves (Favier et al., 2014; Joughin et al., 2014) and the 20th century increase in Antarctic snowfall has been attributed to changes in their circulation (Medley 45 and Thomas, 2019). Sea ice modulates the earth's albedo and governs the area available for exchange of heat and CO_2 between the ocean and the atmosphere. However, records of both westerly winds and sea ice are short, with major uncertainty in the trends prior to the satellite era (i.e. pre 1970's). SAIs on the very margin of maximum winter sea-ice extent could potentially identify local-scale changes in sea ice, rather than relying on ice core records from the Antarctic continent, which record mostly ocean-sector scale trends (Thomas and 50 Abram, 2016; Thomas et al., 2019). An ice core from Bouvet Island, presented in this study, has already proven successful in reconstructing past sea ice variability in the adjacent ocean (King et al., 2019).

Paleoclimate records do exist on some SAIs from lake sediments, peat cores and ice cores. Peat records are currently the most prolific of the three, with a number of records retrieved on the New Zealand SAIs up to 55 12,000 years old (McGlone, 2002) and on Crozet and South Georgia up to 6,000 and 11,000 years old respectively (Van der Putten et al., 2012). One limitation is that annual layers are not preserved in such records and carbon dating carries with it uncertainties in the decadal to centennial range, which complicates the identification of annual to decadal-scale climate variations and the precise timing of climate shifts (Van der Putten et al., 2012). Peat deposits are also lacking on the more southerly SAIs.
60

Lake sediments are similarly useful for studying vegetation composition on the SAIs. These are related to a wide range of environmental parameters within and around the lake used to reconstruct past natural variability (Saunders et al., 2008). Diatom and geochemical proxies from Marion Island have been used to track the migration of westerly winds over the past 700 years (Perren et al., 2020). A novel proxy, based on sea-salt 65 aerosols in lake sediments on Macquarie Island, reconstructed past westerly wind strength over the past 12,300 years (Saunders et al., 2018). However, damage from introduced rabbits at this site has compromised the data during the last ~100 years.

Ice core records offer complementary archives to peat and lake archives on glaciated or ice capped islands' and 70 are in some cases unique records where peat and lake deposits are not available. Shallow ice cores have been drilled from low elevation plateaus and glacial termini on South Georgia, the largest glaciated SAI. The estimated age of the ice at bedrock for the glacial termini sites is between 8,000-12,000 years old (Mayewski et al., 2016). However, surface temperatures on South Georgia have risen by ~1°C during the 20th century (Whitehead et al., 2008) and ninety-seven percent of the 103 coastal glaciers have retreated since the 1950's 75 (Cook et al., 2010). Thus, the valuable paleoclimate archive contained in South Georgia, and potentially the other SAIs glaciers, may be at risk from surface melt.

2

The sub-Antarctic Ice Core drilling Expedition (subICE) was part of the international Antarctic Circumnavigation Expedition (ACE) 2017-2018 (Walton, 2018), which offered an exceptional opportunity to access multiple SAIs. In this study we present the density profiles, melt histories and ground-penetrating radar (GPR) data collected during subICE. These include the first ever firn core records from three of the glaciated Antarctic and SAIs in the Pacific and South Atlantic sector of the Southern Ocean, together with two continental firn cores collected from coastal domes in East and West Antarctica. The aim of this study is to 1) evaluate the firn conditions and internal layering in the upper ice column, 2) determine the extent of surface melt and the potential impact on proxy preservation 3) estimate potential bottom ages for future deep drilling expeditions.

2 Methods and Data

2.1 Firn cores

Six firn cores were drilled as part of subICE, between January and March 2017 (Table. 1). The teams were deployed to the sites via helicopter from the ship (Akademik Tryoshnikov), allowing between three and eight hours of drilling time, dependent on weather conditions and logistical capability. The firn cores were drilled using a Mark III Kovacs hand-auger with sidewinder winch and powerhead, retrieving sections of approximately 70 cm in length. The firn was measured, placed inside pre-cut layflat tubing and packed in insulated ice core storage boxes for transportation. During the voyage, the ice was stored in a -25°C freezer and later transported to the ice core laboratories at the British Antarctic Survey (BAS).

2.2.1 Bouvet Island (Bouvetøya)

A 14 m firn core was drilled from the volcanic island of Bouvet in the central South Atlantic (54°26'0 S, 3°25'0 E, 50 km²), also known as Bouvetøya (Figure 1a). This was the most northerly site but the island's location within the polar front (Figure 1) classifies it as sub-Antarctic.

Bouvet is almost entirely ice covered (~50 km²) except for a few rocky outcrops around the coast. Ice flows down the flanks of the volcano, with no visible crevassing, giving way to shear ice-cliffs and near-vertical icefalls into the sea. The island is the southernmost extension of the mid-Atlantic ridge, located at the triple junction between the African, South American and Antarctic plates. These pronounced sea floor features drive the cold Antarctic Circumpolar Current close to the island, keeping surface temperature cold and allowing sea ice to extend north of the island.

The last known volcanic eruption on Bouvet was 50 BC; however, visible ash and dust layers suggest eruptions may be more frequent. At several locations, the ice edge has broken vertically away (Figure S1) revealing horizontal bands of clean and dirty layers in the vertical stratigraphy. The islands remote location, and absence of significant local dust sources, suggests a local volcanic source from either Bouvet or the South Sandwich Islands. The 3.5 km wide Wilhelmplataet caldera appears entirely ice filled. This potentially offers the deepest coring location; however, it is unclear if this is instead an ice bridge formed since the last eruption.

2.1.2 Peter 1st Island

3

A 12 m firn core was drilled from Peter 1st Island (68°50'0 S, 90°35'0 W), in the Bellingshausen Sea (Figure 1b). The former shield volcano (154 km^2) is almost completely covered by a heavily crevassed ice cap and sits within the seasonal sea ice zone. The core was drilled on a ridge (Midtryggen) at 730 m above sea level (a.s.l), 120 in a small saddle on the eastern side of the island overlooking the main glacier Storfallet.

2.1.3 Mount Siple

A 24 m firn core was drilled on Mount Siple (73°43'S, 126°66'W) on the Amundsen Sea coast, West Antarctica (Figure 1c). Mount Siple is an active shield-volcano rising to 3,110 m a.s.l at its peak from Siple Island on the 125 coast of Marie Byrd Land, surrounded by the Getz ice shelf. The core was drilled at 685 m a.s.l

2.1.4 Young Island

A 17 m firn core was drilled on Young Island (66°17′S, 162°25′E), the northernmost island in the Balleny Island chain (245 km^2), off the coast of Adélie Land (Figure 1d). The Balleny Islands comprise three major dormant 130 volcanic islands, Young, Buckle and Sturge (Hatherton et al., 1965), which sit in the Antarctic seasonal sea ice zone at the boundary of the polar westerlies and Antarctic coastal easterlies. Young Island is characterized by a thick ice cover, marine-terminating piedmont-glacier tongues, steep coastal cliffs, and is therefore described as "among the most inaccessible places in the world" (Hatherton et al., 1965). The core was drilled 238 m a.s.l.

135 2.1.5 Adelie Land Coast (Mertz)

Two firn cores were drilled on the coast of Adélie Land in East Antarctica (Figure 1e); a 20 m core (Mertz 1) from Cape Hurley, a low elevation ice dome on the eastern side of the Mertz Glacier (67° 33' S, 145° 18' E); and a 9 m firn core (Mertz fast ice) drilled on a triangular wedge of fast ice in Fisher Bay (67° 26' S, 145° 34' E), bounded on the east by the Mertz Glacier and on the west by the AAE (Australian Antarctic Expedition) glacier.

140

The Mertz Glacier extends into the ocean from coastal King George V land, with a floating ice tongue. The tongue traps pack ice upstream forming the Mertz Glacier Polynya along its western flank during winter, the third most productive polynya in Antarctica, (Lacarra et al., 2014). In 2010, the impact from the B9B iceberg caused this tongue to calve off producing a ~80 km long iceberg. This event had a profound impact on local sea 145 ice conditions and the formation of dense shelf water (Campagne et al., 2015).

2.2 Firn core analysis

Firn-core analysis was carried out in the -20°C cold laboratories at BAS. The section length, diameter and weight were measured to provide a density and the visible melt layers logged and measured (only layers > 150 1mm).

2.3 Ground-Penetrating Radar

GPR measurements were performed around each firn core site. We used a SIR3000 unit equipped with a 400 MHz central frequency antennae (GSSI Inc.). The system was pulled on a sledge while walking in parallel and transversal lines of 100 m to 500 m depending on the site surface conditions and available time at each site. The 155 penetration depth of the propagated wave is strongly controlled by the electrical properties of the subsurface

combined with the central frequency of the system. The equipment used provides a good compensation between these parameters in polar snow. Vertical resolution is approximately 0.35 m, reaching up to 100 m depth in very dry snow (ideal conditions), such as in the Antarctic plateau (Spikes et al., 2004). However, the resolution and maximum reachable depth are expected to decrease dramatically at lower latitudes. This GPR was intended to obtain data from the near surface (up to 40 m) to complement the firn-core observations and to better characterise the stratigraphy of each site.

The data collected (radargram) represent the number of traces received (x-axis) and the two-way travel time of the wave in nano seconds (ns) (y-axis), which is the time the signal takes from the transmitter to the receiver when reflected from the internal ice discontinuities (melt layers). During data collection the maximum time window was set to a value between 400 – 600 ns, according to the expected maximum depth of signal propagation at the SAI sites. GPR data was monitored in-situ for calibration and stored. Data processing was done using a commercial software (ReflexW) and included: removal of repetitive traces (same position), correction of the surface position and distance covered, frequency filters, gain function adjustments, stacking and other visual enhancements to improve the interpretation of the reflecting layers. Each collected file was analysed independently, and layers picked manually in full resolution. If layers were not sufficiently clear and continuous, they were not picked.

We used the density profile (see section 3.3) of the firn core to obtain dielectric values through depth, based on the Looyenga model (Looyenga, 1965), and estimated the wave velocity variations and corresponding depth of the layers..

2.4 Meteorological data

Meteorological data come from the European Centre for Medium-Range Weather Forecasts (ECMWF) ERA-5 analysis (1979–2017) (Copernicus Climate Change Service, 2017), the fifth generation of ECMWF reanalysis. ERA-5 reanalysis currently extends back to 1979, providing hourly data at 0.25°resolution (~ 31 km). Annual average precipitation minus evaporation (P-E) and maximum monthly temperatures (1979-2017) are presented in Table 1. We note that the resolution of ERA-5 is currently unable to capture local climate conditions on the SAIs, however, a recent study from the Antarctic Peninsula confirmed its high accuracy in representing the magnitude and variability of near-surface air temperature and wind regimes (Tetzner et al., 2019).

Limited in-situ meteorological observations are available from the University of Wisconsin-Madison Antarctic Meteorology Program and the Norwegian Polar Institute Automatic weather station (AWS) data are available from Bouvet Island (April 1997-December 2005), Peter 1st Island (September 2006 to January 2007, not complete), Mount Siple (January 1992 to January 2015) and Young Island (January 1991 to December 1997).

The 2 m temperature from ERA-5 (Figure 1) and the AWS sites (typically at low elevations) are expected to be warmer than the firn core drilling locations, as a result of the adiabatic rate of temperature change for vertically moving air. This lapse rate varies with both temperature and mixing ratio from a dry rate of 0.98°/100 m to a saturated rate of 0.44°/100 m at 20°C (Martin and Peel., 1978). As a best guess, we use a lapse rate of 0.68°/100

5

195m to calculate the temperature at the drilling sites. This value is observed on the western Antarctic Peninsula (Martin and Peel., 1978), where the climate and maritime conditions are expected to closely resemble those of the SAIs.

3 Results

200**3.1 GPR**

Given the scope of this paper, one example of a representative profile taken near the firn core is shown in the following section. Figures 2-5 show a) a reference map of the track of measurements, b) a section of the radargram and c) the estimated depth (up to 20 m) of the picked layers considering the variations of the propagation velocity given the density profile.

205

3.1.1 Bouvet Island

GPR data obtained at Bouvet island generally show layers of accumulated snow. The reference map (Figure 2a) shows the selected profile (grey line) descending from 357 m a.s.l. to 339 m a.s.l towards the south east. Figure 2b shows the interpreted layers observed near the firn core extraction site. The estimated depth of the layers 210shows that there is about 2 m of horizontal continuous layering of snow. Below this layer, there is stratified firn that have been eroded by the effect of wind and the surface slope, reaching a layer of solid ice at 15 m from the surface. Another layer is detected at 36 m depth, which is interpreted as the bedrock. This depth is consistent with the estimated ice thickness observed from the ice cliffs to the south of the firn core drilling site (Figure S1). Ice thickness from the photograph is estimated relative to the expected size of the observed fur seals on the 215beach.

3.1.2 Peter 1st Island

Snow surface at Peter 1st site was smooth (maximum 5° slope). Internal layers were only (and partially) traceable for the upper ~25 m of the snow/firn pack. The maximum time window was set to reach an estimated depth of ~43 m (Table 2) and bedrock was not detected. Figure 3a shows the track of measurements performed 220at Peter 1st island site and the profile shown (Figure 3b) is a section of the line (grey line) taken at increasing elevation from 718 m a.s.l. up to 726 m a.s.l. in a north-westerly direction. Figure 3c shows the estimated depth for the stratified layers of snow in the upper 14 m were mostly continuous.

3.1.3 Mount Siple

225The surface of the studied area at Mount Siple site was relatively smooth (max. 4° slope). Figure 4a shows the length and position of a full profile taken in a south-westerly direction taken in an east-westerly direction rising from 678 m a.s.l. to 685 m a.s.l. and ending at the firn core extraction position. Figure 4b shows the selected section where clear layering can be observed for the upper 20 m with smooth depth variation through the profile length. Bedrock was not detected.

230

3.1.4 Young Island

The Young Island site surface was flat with a compact snow. The maximum estimated depth of detected layers was ~36 m (Table 2) and bedrock was not detected. Figure 5b shows a section of a selected profile taken in a

6

north-westerly direction starting at the firn core extraction position, here multiple layers can be identified but they are discontinuous and the small distance between layers resulted in merging, thus they are not traceable through the full profile length.

3.1.5 Adelie Land Coast (Mertz)

The Mertz 1 site (Cape Hurley) had a flat surface, consistent with observed internal layering. Layers could not be distinguished in the upper ~7 m of snow and only reflected weakly beneath this depth; 11 distinct, but discontinuous, layers were identified down to a depth of 62 m (bedrock was not detected). We estimated this to be the approximate limit of signal propagation of the GPR system at this site. Figure 6 a-c shows a section of a profile taken in north westerly direction and the interpretation of layers depth in the upper 20 m near the firn core extraction.

Data quality for the Mertz fast ice site was very poor (Figure 6 d-e). A single continuous layer at 6.8 m depth was the only one identified.

3.2 Melt records

Given their location, we expect all sites to experience some degree of surface melt. The elevation corrected temperature for each SAI is compared with the 2 m temperature and uncorrected AWS temperature in Table 1. Surprisingly, the site least affected by melt is Bouvet, the warmest and most northerly location. Despite its northerly location the average yearly temperature from ERA-5 (elevation corrected) is -2.9 °C, with a maximum monthly temperature of -0.9°C. The maximum value recorded by the AWS at 42 m.a.s.l was 6.7 °C (1997-2005, elevation corrected). The average melt layer thickness in the Bouvet core is 0.3 cm, observed at a frequency of five layers per meter; with the largest measured melt layer just 3.95 cm (Table 2).

The coldest site is Mertz Glacier, with an annual average temperature (ERA-5 elevation corrected) of -17.4°C. The percentage of melt at this site is just 6%, with a maximum layer thickness of 8.1 cm. The melt layer thickness at the Mertz fast ice site appears to be lower, however, this only reflects visible melt layers in the top 2.2 m.

Average melt layer thickness at Peter 1st Island is comparable to that of Mount Siple, with percentage melt of 11% and 10% respectively. Reflecting the similar summer temperatures, -5.1°C at Peter 1st and -5.2°C at Mount Siple.

The site most affected by melt is Young Island, which has frequent melt layers averaging 6.57 cm and the largest single layer of 58 cm. The annual average temperature from this site is -9.2°C, (ERA-5 1979-2017), with a maximum AWS temperature of 2.8°C (February 1997). Melt layers occur throughout the profile but with greatest density between 5–5.5 m and below 11 m depth. Most melt layers consist of bubbly ice with a minority of thinner layers that are bubble-free or exhibit large crystals. We note that the visual method of determining

7

melt layers is not sufficient to determine if the large layers result from individual melt events or are formed from a sequence of smaller events.

3.3 Relationship between GPR horizons and firn core melt layers

In order to explore the spatial extent of melt surrounding the firn core sites, we compare the firn core melt records with the GPR horizons. However, the melt observations from the firn core have a resolution of 1mm, while the 400 MHz antenna provides a range of visibility of ~35 cm for the dielectric permittivity values at these firn conditions (Koppenjan, 2009; Arcone, 2009). Thus, we first reduce the resolution of the firn core derived melt profiles by summing the total melt in a running 35 cm window. Only sections that would produce a strong enough (visible in the profiles at full resolution) reflection to be detected by the GPR are included in the comparison. The continuity of the GPR data has been assessed in profile sections of 20 m length near the firn core extraction (plot c in Figures 2-6) and their mean depth have been used. Subsequently, we compared the potentially visible patterns from the firn core to the depth of the handpicked layers in the radargrams (Figure 7).

3.4 Density

The change in firn density with depth is dependent on the snow accumulation rate and temperature at the site. Higher temperature and lower accumulation rates result in the greatest change of density with depth. At our sites the depth-density profile exhibits more variability at the island sites (Bouvet, Peter 1st, Young) than the continental sites (Mertz and Mount Siple), reflecting the warmer island locations and the influence of surface melt (Figure 8).

A fitted density curve is applied based on the assumption that firn densification is linearly related to the weight of overlying snow (Herron and Langway, 1980). The density with depth (ph) is calculated following Eq. (1):

$$ph=p_i\text{-exp (ln a }+b)\tag{1}$$

where p is the density, p_i is the density of ice (0.917 kg m^{-3}) and h is the snow depth. The constants a and b are derived from the linear relationship between ln $[p/(p_i\text{-}p)]$ and depth, where ln(a) is the intercept, and b is the gradient. The first stage of densification relates to grain settling and packing and occurs below the "critical density" of about 0.55 kg m^{-3} (Herron and Langway, 1980). The second stage of densification (0.55–0.83 kg m^{-3}), occurs when the firn air passages become closed off to form individual bubbles. The critical depth (zero-intersection) and the close off depth at each site is presented in Table 3.

3.5 Estimating the firn core bottom ages

The fitted density curve can provide a first approximation of the age-scale (Table 3), based on the (water-equivalent) annual average P-E from ERA-5. We note that the resolution of ERA-5 may not be adequate to capture P-E at these sites and that snow accumulation may vary through time. It would have been preferable to use a densification model that accounts for the influence of melt (e.g. Lightenberg et al., 2011), however the current in-situ observations at these sites do not allow for this. Thus, our approach is very simplified with the aim of establishing a preliminary bottom age for each site.

8

310In the Herron and Langway densification model the dominant densification process in the upper part ($\rho \leq 550$ kg m−3) are grain settling and packing of snow grains (Herron and Langway, 1980). Undoubtably, refreezing of melt water and/or liquid precipitation also cause firn to densify. This is observed in figure 8, as jumps in the measured density corresponding to large melt events. However, if we assume that heat is released upon refreezing, the local firn temperature will also increase, further accelerating the densification. At the same time, 315ice layers lead to a higher average density, thereby reducing the potential densification rate. Although not ideal, the measured density value used in the equation will reflect the presence of melt. As such, the values of surface snow (or zero-intersection depth) are considerably higher than those modelled or observed for coastal Antarctica (van den Broeke, 2008).

320We apply an error estimate to the bottom ages to account for the potential influence of melt, changing snow accumulation with time and uncertainties in the ERA-5 P-E value. This is based on the difference between the age determined using the mean annual P-E value and the age determined when using an upper (annual P-E plus one standard deviation) or lower (annual P-E minus one standard deviation) P-E value. The error variability reflects the variability in precipitation at each site and increases with depth and age.
325

For the sites where bedrock was not detected, we estimate the bottom age of an ice core drilled to 100 m depth (Table 3). This suggests that the oldest ice would be reached at Mertz 1 (1849 +/- 64 years) and the youngest ice at Mount Siple (1912 +/- 35 years).

3304 Discussion

Based on the results we aim to establish which of the sites would be suitable for future deep drilling expeditions, based on 1) the firn conditions and internal layering in the upper ice column, 2) the extent of surface melt and the potential impact on proxy preservation, and 3) potential bottom ages.

3354.1 Firn conditions and internal layering in the upper ice column

4.1.1 Density

A linear relationship exists between the 2-m temperature from ERA-5 and the critical depth ($r^2 = 0.57$, $p>0.05$), which is reached first at Bouvet, the most northerly location and the warmest site (Table 1; Table 3). Young Island is the only site where the close-off depth is reached, which exceeds this density threshold (0.83 kg m^{-3}) at 34016.6 m. This suggests that pore close-off has been achieved, when air can no longer be excluded and further densification takes place by compression of the bubbles. However, the presence of a large melt layer at this depth suggests this may be the cause of the density increase. Based on the fitted density profile the actual close-off depth occurs at 21 m. The second fastest close-off depth occurs at Bouvet (28.65 m), considerably shallower than the two coastal Antarctic sites (Mount Siple and Mertz 1).

345Surface densities, critical depths and close-off depths at the continental sites (Mount Siple and Mertz 1) are consistent with modelled values (van den Broeke, 2008). A compilation of observed (and modelled) Antarctic snow densities suggest a range of 6- 26 m (modelled 4-29.5 m) for the critical depth and 34-115 m (modelled

9

45-115 m) for pore close-off. The values for Bouvet, Peter 1st and Young Island are close to the modelled values for coastal Antarctica, however, the pore close-off depth at both Bouvet and Young Island is achieved faster than the lowest reported depth for an Antarctic site (34 m at Upstream B, West Antarctica)(van den Broeke, 2008). The presence of melt layers, with a greater density than the surrounding firn, may bias our close-off estimates to shallower depths. In addition to the influence of temperature, the rapid densification on the SAIs may be caused by layer stretching and compression related to ice flow that is not well understood at these locations.

4.1.2 GPR

The aim of the GPR data was to give a preliminary characterisation of each site, particularly the distribution, continuity and clearness of the horizons observed in this data. Bouvet was the only site where bedrock was detected, suggesting that the maximum depth of an ice core from this site is ~40 m. Evidence of wind scouring in the reflections may impact the proxy preservation at this site. The profiles at Peter 1st, Mount Siple and Mertz indicate more uniform internal structure, with traceable layers in the top 20 m. The largest number of layers was identified at Young Island, but many were discontinuous or difficult to trace. The deepest layer detected was at Mertz, the coldest site, where layers were traceable to a depth of 62 m.

4.1.3 Case study Mertz fast ice

This Mertz fast ice site is fundamentally different in character from the others presented in this study. While we believe the surface snow to be meteoric, it does not sit atop grounded ice, but rather a large wedge of multiyear sea ice, held fast between the AAE and Mertz Glacier tongues (Figure 1d). The top-most layers of snow and firn appeared typical of surface snow. However, at a drill depth of 6.23 m the core was saturated with liquid seawater (a strong attenuator of the radar signal). Ice recovered below this depth was different in character from the surface, being solid ice containing bubbles and interstitially saturated with saltwater. There was a standing water table in the borehole at this same depth. These observations, together with the clear radar reflector at just over 6.8 m (Figure 6), the absence of reflectors below this, and the site's elevation of ~6 m.a.s.l, lead to the conclusion that the fast ice is saturated with seawater below sea level.

If the fast ice is floating (i.e. supported buoyantly), our measurement of the dry freeboard thickness allows us to estimate the total thickness of the fast ice wedge. The average density of the top 6 m is 0.55 +/- 0.05 kg m^{-3}, increasing to 0.85 +/- 0.05 kg m^{-3} below this. Assuming a seawater density of 1.0275 ± 0.004 kg m^{-3}, freeboard thickness of 6.2 m and a mean density of the ice below the water-table of 0.85 +/- 0.05 kg m^{-3}, the total ice-equivalent thickness of the ice at this site is ~30 m. However, there are large uncertainties in this calculation. The radargram indicates that the fast ice increases in thickness away from the drill site, by several meters. While this site is not likely to provide typical geochemical proxy records, it may be of interest to future studies of multiyear sea ice.

4.2 Extent of surface melt and the potential impact on proxy preservation

4.2.1 Melt recorded in the firn core

Surface melting occurs in response to a positive energy balance at the snow surface and is strongly correlated with surface air temperature. The Antarctic ice sheet experiences little melt, due to consistently low temperature,

10

however the coastal margins and areas of the Antarctic Peninsula are subject to surface melting (van Wessem et al., 2016). The relationship between surface melt and surface temperature has been exploited to reconstruct past climate in Antarctic ice cores (Abram et al., 2013). However, the presence of too much surface melt can damage the climate proxies they contain.

390

The influence of melt-water on ice core proxy preservation has been explored for Arctic ice cores (Koerner, 1997). Here, melt-water percolation can allow insoluble micro particles to migrate to the melting surface, causing a spike in concentrations, and influence the stable water isotope record, a commonly used proxy for past surface temperature. Seasonal melting can cause run-off of near-surface snow and melt and refreezing at the 395 base of the annual snowpack. This can redistribute the stable water isotope profile, resulting in a warm or cold-biased record. The influence on both stable water isotopes and chemistry can have a major impact on the ability to date ice cores using annual layer counting. The site most affected by melt is Young Island, with 47% of the firn core characterised as melt. Given the islands location south of the Polar Front and the seasonal sea ice zone (Figure 1) the evidence of extensive surface melting is unexpected. Especially when considering that the 400 average temperature at Young Island is 6.4° colder than Bouvet, the site least affected by melt. It is likely that the resolution of ERA-5 is not sufficient to capture local surface temperature, however, the 3-hourly data from the AWS (1993-1997) reveals considerable variability.

The maximum temperature recorded by the Young AWS (elevation corrected) is 2.8°C (February 1997), with temperatures in 20 of the 67 months of AWS data exceeding 0°C. The annual average temperature at Young 405 Island is comparable with Peter 1st, with a lower maximum AWS temperature. However, the largest melt layer at Young is almost twice that of Peter 1st and the percentage melt over four times higher. Solar radiation is the dominant driver of surface melting although atmospheric thermodynamics and cloud radiative properties also play a role. Thus, our study demonstrates that for the SAI's surface temperature alone is not a reliable indicator of potential melt damage.

410 The average melt layer thickness at all sites (except Young Island) is considerably lower than the mean melt layer width of 3.2 cm observed at the James Ross Island ice core, from the northern Antarctic Peninsula (Abram et al., 2013). The percentage of melt per year is dependent on the measured snow accumulation. The estimated snow accumulation at Bouvet is 0.59 m water equivalent, based on annual layer counting of chemical and isotopic species (King et al., 2019b). The annual layer counting of the other subICE cores has not yet been 415 completed, however based on our estimates (section 3.4), it is a reasonable assumption that the snow accumulation at these maritime islands will be equal to or more than the snow accumulation at James Ross Island (0.62 +/- 0.14 m water equivalent). Thus, the potential for proxy preservation and climate reconstructions is promising at these sites.

420 Given the degree of melt at Young Island, it seems likely that the proxy preservation may be compromised. However, an evaluation of the firn/ice microstructure may help determine the extent to which melt water has percolated through the layers.

11

4.2.2 Comparison of firn core melt with GPR layers

425 There appears to be little correlation between the melt observed in the core and the layers traced in the GPR. The relationship is particularly poor for Young Island, where the core shows a high amount of thin melt layers seen in the radar data as very dense non-continuous layering. Although it is not possible to determine the spatial extent of melting based on the GPR profiles, the findings suggest that density variations alone cannot explain the internal layering.

430 The presented comparison method is subject to several sources of uncertainty. 1) The manual picking of the GPR layer, 2) the distance between the firn core extraction point and the section of the radar data, and 3) the use of average depth in sections of 20 m distance, especially for the sites that exhibit an incline (e.g. Bouvet and Mount Siple).

435 4.3 Potential bottom ages of deeper ice cores

One of the aims of this study was to establish the SAI's suitability for future deep ice core drilling projects. A useful indicator is the potential bottom age at each site. The estimated firn core bottom ages range from 2004 (+/-3 years), at both the Peter 1st and Bouvet firn cores, to 1994 (+/- 8 years) at Mertz 1 (Table 3).

440 To date, only the Bouvet firn core has been independently dated. Annual layer counting, using a suite of chemical and isotopic species, yielded a bottom age of 2001 AD (King et al., 2019). Although older than the bottom age estimate using the density profile it is within error (2004 +/- 3 years) adding confidence to this approach but suggesting our ages may be too conservative. The offset may be explained by an over-estimate in the P-E derived from ERA-5 or suggest the influence of post-depositional processes such as wind scouring or 445 ablation.

It is difficult to estimate a potential age limit for a core drilled to bedrock at the Young, Peter 1st and Mertz 1 sites since the ice thickness was beyond the penetration depth of the GPR. For example, at Mertz 1 a bottom age of 1926 AD (+/- 34 years) is estimated based on a GPR bottom depth of 63 m (Table 2), although the ice could 450 feasibly be much deeper than this. At the Bouvet site, where we interpret the layer at ~40 m as bedrock, the maximum potential age is 1971 AD (+/- 11 years). However, considerably deeper (and therefore older) ice may be present at higher elevations. These results suggest that the subICE firn-core records will be suitable for obtaining sub-annual resolution climate records with the potential to capture climate variability over multi-decadal timescales.

455

The estimated firn core bottom age at Bouvet Island, together with the observed visible ash layers (Figure S1), offer a glimpse at the volcanic history of this remote island. The last known eruption was 50 BCE; however, visible layers in the upper ~20 m suggest the island has been volcanically active as recently as ~ 1998. The regularity of the layers in the ice cliffs, visible all around the island, indicate frequent volcanic activity has 460 occurred during the 20th century. This is consistent with the persistent volcanic activity observed on the near-by South Sandwich Islands, with visible ash clouds identified in the satellite records and even visible from the ship during the ACE (March 2017). We note that the visible ash layers at Bouvet (Figure S1) may have been deposited from the South Sandwich Islands but further analysis will help establish the source.

12

5 Conclusions

Initial results from five shallow firn cores drilled in the sub-Antarctic islands and coastal Antarctica suggest that these locations may be suitable for short-term climate reconstructions and up to centennial-scale reconstructions at some sites if deeper cores could be retrieved. Evidence that these firn cores span the 20th century, a period of significant global climate change, is exciting. The GPR surveys suggest relatively uniform layering at most sites, at least to the depth of the firn cores, suitable for firn core proxy reconstructions. However, evidence of crevassing at some locations (Young and Peter 1st) demonstrates the importance of a thorough geophysical survey before contemplating deeper drilling at these sites. At Bouvet Island, regular volcanic ash deposits during the 20th century suggest the island is still volcanically active.

The impact of melt is less severe than expected at some locations, especially Bouvet Island, but more severe at others. Young Island, part of the Balleny Island chain off the coast of Adèlie Land, is the most susceptible to melt. However, the observed melt layer thickness at the other sites is less than that observed from the James Ross Island ice core, which yielded paleoclimate reconstructions (Abram et al., 2013). Proxy preservation was not a concern in this ice core, suggesting that melt will also not adversely influence the climate record contained in the sub-Antarctic firn cores. The observed increase in melt intensity at James Ross Island since the mid-20th century was linked to warming surface temperature. Thus, the comparable melt intensity observed at some of the SAIs may be evidence that the 20th century warming at these locations was analogous to that on the Antarctic Peninsula.

Based on the measured density profile and the P-E from ERA-5, the estimated bottom ages of the subICE cores range from 2004 (Peter 1st and Bouvet) to 1994 (Mertz 1), suggesting that these records should contain a multi-decadal record of climate variability in this data sparse region. We were unable to obtain ice thickness estimate for all sites, with the exception of Bouvet, however visible layers were identified in the GPR records to depths of 60 m. Even with a conservative estimate, it is possible that deeper ice cores drilled on these SAIs would have the potential to capture climate variability during the 20th century, but most likely considerably longer.

13

References

520 Abram, N.J., Mulvaney, R., Wolff, E.W., Triest, J., Kipfstuhl, S., Trusel, L.D., Vimeux, F., Fleet, L. and
Arrowsmith, C., 2013. Acceleration of snow melt in an Antarctic Peninsula ice core during the
twentieth century. Nature Geoscience, 6(5): 404-411.

Arcone, Steven. (2009). Glaciers and Ice Sheets. In H. Jol (Ed.), Ground Penetrating Radar Theory and
Applications (pp.361-392). Oxford: Elsevier

525 Campagne, P., Crosta, X., Houssais, M.N., Swingedouw, D., Schmidt, S., Martin, A., Devred, E., Capo, S.,
Marieu, V., Closset, I. and Massé, G., 2015. Glacial ice and atmospheric forcing on the Mertz Glacier
Polynya over the past 250 years. Nature Communications, 6(1): 6642.

Cook, A.J., Poncet, S., Cooper, A.P.R., Herbert, D.J. and Christie, D., 2010. Glacier retreat on South Georgia
and implications for the spread of rats. Antarctic Science, 22(3): 255-263.

530 Copernicus Climate Change Service (C3S) (2017): ERA5: Fifth generation of ECMWF atmospheric reanalyses
of the global climate . Copernicus Climate Change Service Climate Data Store (CDS), February 2020.
https://cds.climate.copernicus.eu/cdsapp#!/home

Cullather, R.I., Bromwich, D.H. and Van Woert, M.L., 1998. Spatial and Temporal Variability of Antarctic
Precipitation from Atmospheric Methods. Journal of Climate, 11(3): 334-367.

535 Emile-Geay, J., McKay, N.P., Kaufman, D.S., von Gunten, L., Wang, J., Anchukaitis, K.J., Abram, N.J.,
Addison, J.A., Curran, M.A.J., Evans, M.N., Henley, B.J., Hao, Z., Martrat, B., McGregor, H.V.,
Neukom, R., Pederson, G.T., Stenni, B., Thirumalai, K., Werner, J.P., Xu, C., Divine, D.V., Dixon,
B.C., Gergis, J., Mundo, I.A., Nakatsuka, T., Phipps, S.J., Routson, C.C., Steig, E.J., Tierney, J.E.,
Tyler, J.J., Allen, K.J., Bertler, N.A.N., Björklund, J., Chase, B.M., Chen, M.-T., Cook, E., de Jong, R.,
540 DeLong, K.L., Dixon, D.A., Ekaykin, A.A., Ersek, V., Filipsson, H.L., Francus, P., Freund, M.B.,
Frezzotti, M., Gaire, N.P., Gajewski, K., Ge, Q., Goosse, H., Gornostaeva, A., Grosjean, M., Horiuchi,
K., Hormes, A., Husum, K., Isaksson, E., Kandasamy, S., Kawamura, K., Kilbourne, K.H., Koç, N.,

14

Leduc, G., Linderholm, H.W., Lorrey, A.M., Mikhalenko, V., Mortyn, P.G., Motoyama, H., Moy, A.D., Mulvaney, R., Munz, P.M., Nash, D.J., Oerter, H., Opel, T., Orsi, A.J., Ovchinnikov, D.V.,

545   Porter, T.J., Roop, H.A., Saenger, C., Sano, M., Sauchyn, D., Saunders, K.M., Seidenkrantz, M.-S., Severi, M., Shao, X., Sicre, M.-A., Sigl, M., Sinclair, K., St. George, S., St. Jacques, J.-M., Thamban, M., Kuwar Thapa, U., Thomas, E.R., Turney, C., Uemura, R., Viau, A.E., Vladimirova, D.O., Wahl, E.R., White, J.W.C., Yu, Z., Zinke, J. and Consortium, P.A.k., 2017. A global multiproxy database for temperature reconstructions of the Common Era. Scientific Data, 4(1): 170088.

550 Favier, L., Durand, G., Cornford, S.L., Gudmundsson, G.H., Gagliardini, O., Gillet-Chaulet, F., Zwinger, T., Payne, A.J. and Le Brocq, A.M., 2014. Retreat of Pine Island Glacier controlled by marine ice-sheet instability. Nature Climate Change, 4(2): 117-121.

Hatherton, T., Dawson, E.W. and Kinsky, F.C., 1965. Balleny Island's Reconnaissance Expedition, 1964. New Zealand Journal of Geology and Geophysics, 8(2): 164-179.

555 Herron, M.M. and Langway, C.C., 1980. Firn Densification: An Empirical Model. Journal of Glaciology, 25(93): 373-385.

Joughin, I., Smith, B.E. and Medley, B., 2014. Marine Ice Sheet Collapse Potentially Under Way for the Thwaites Glacier Basin, West Antarctica. Science, 344(6185): 735.

King, A.C.F., Thomas, E.R., Pedro, J.B., Markle, B., Potocki, M., Jackson, S.L., Wolff, E. and Kalberer, M.,

560   2019. Organic Compounds in a Sub-Antarctic Ice Core: A Potential Suite of Sea Ice Markers. Geophysical Research Letters, 46(16): 9930-9939.

Koerner, R.M., 2017. Some comments on climatic reconstructions from ice cores drilled in areas of high melt. Journal of Glaciology, 43(143): 90-97.

Koppenjan, S. (2009). Ground Penetrating Radar Systems and Design. In H. Jol (Ed.), Ground Penetrating

565   Radar Theory and Applications (pp.73-97). Oxford: Elsevier

Lacarra, M., Houssais, M.-N., Herbaut, C., Sultan, E. and Beauverger, M., 2014. Dense shelf water production in the Adélie Depression, East Antarctica, 2004–2012: Impact of the Mertz Glacier calving. Journal of Geophysical Research: Oceans, 119(8): 5203-5220.

Ligtenberg, S. R. M., Helsen, M. M., and van den Broeke, M. R., 2011. An improved semi-empirical model for

570   the densification of Antarctic firn, The Cryosphere, 5, 809–819, https://doi.org/10.5194/tc-5-809-2011.

Looyenga, H., 1965. Dielectric constants of heterogeneous mixtures. Physica, 31(3): 401-406.

Martin, P., & Peel, D. (1978). The Spatial Distribution of 10 m Temperatures in the Antarctic Peninsula. Journal of Glaciology, 20(83), 311-317. doi:10.3189/S0022143000013861

Mayewski, P.A., Kuli, A., Casassa, G., ArÉValo, M., Dixon, D.A., Grigholm, B., Handley, M.J., Hoffmann, H.,

575   Introne, D.S., Kuli, A.G., Potocki, M. and Sneed, S.B., 2016. Initial reconnaissance for a South Georgia ice core. Journal of Glaciology, 62(231): 54-61.

McGlone, M.S., 2002. The Late Quaternary peat, vegetation and climate history of the Southern Oceanic Islands of New Zealand. Quaternary Science Reviews, 21(4): 683-707.

Medley, B. and Thomas, E.R., 2019. Increased snowfall over the Antarctic Ice Sheet mitigated twentieth-

580   century sea-level rise. Nature Climate Change, 9(1): 34-39.

Nye, J.F., 1963. Correction Factor for Accumulation Measured by the Thickness of the Annual Layers in an Ice Sheet. Journal of Glaciology, 4(36): 785-788.

15

Perren, B.B., Hodgson, D.A., Roberts, S.J. et al. Southward migration of the Southern Hemisphere westerly winds corresponds with warming climate over centennial timescales. Commun Earth Environ 1, 58 (2020). https://doi.org/10.1038/s43247-020-00059-6

Pendlebury, S., Barnes-Keoghan, IP 2007. Climate and climate change in the sub-Antarctic. Papers and Proceedings of the Royal Society of Tasmania, vol. 141, no. 1 pp. 67-81.

Saunders, K.M., Hodgson, D.A. and McMinn, A., 2008. Quantitative relationships between benthic diatom assemblages and water chemistry in Macquarie Island lakes and their potential for reconstructing past environmental changes. Antarctic Science, 21(1): 35-49.

Saunders, K.M., Roberts, S.J., Perren, B., Butz, C., Sime, L., Davies, S., Van Nieuwenhuyze, W., Grosjean, M. and Hodgson, D.A., 2018. Holocene dynamics of the Southern Hemisphere westerly winds and possible links to CO2 outgassing. Nature Geoscience, 11(9): 650-655.

Spikes, V.B., Hamilton, G.S., Arcone, S.A., Kaspari, S. and Mayewski, P.A., 2004. Variability in accumulation rates from GPR profiling on the West Antarctic plateau. Annals of Glaciology, 39: 238-244.

Tetzner, D., Thomas, E. and Allen, C., 2019. A Validation of ERA5 Reanalysis Data in the Southern Antarctic Peninsula—Ellsworth Land Region, and Its Implications for Ice Core Studies. Geosciences, 9(7): 289.

Thomas, E.R., Allen, C.S., Etourneau, J., King, A.C.F., Severi, M., Winton, V.H.L., Mueller, J., Crosta, X. and Peck, V.L., 2019. Antarctic Sea Ice Proxies from Marine and Ice Core Archives Suitable for Reconstructing Sea Ice over the Past 2000 Years. Geosciences, 9(12): 506.

van den Broeke, M., 2008. Depth and Density of the Antarctic Firn Layer. Arctic, Antarctic, and Alpine Research, 40(2): 432-438, 7.

Van der Putten, N., Mauquoy, D., Verbruggen, C. and Björck, S., 2012. Subantarctic peatlands and their potential as palaeoenvironmental and palaeoclimatic archives. Quaternary International, 268: 65-76.

van Wessem, J.M., Ligtenberg, S.R.M., Reijmer, C.H., van de Berg, W.J., van den Broeke, M.R., Barrand, N.E., Thomas, E.R., Turner, J., Wuite, J., Scambos, T.A. and van Meijgaard, E., 2016. The modelled surface mass balance of the Antarctic Peninsula at 5.5 km horizontal resolution. The Cryosphere, 10(1): 271-285.

Walton, D., Thomas. J., 2018. Cruise Report - Antarctic Circumnavigation Expedition (ACE) 20th December 2016 - 19th March 2017 (Version 1.0). Zenodo. http://doi.org/10.5281/zenodo.1443511.

Whitehead, H., McGill, B. and Worm, B., 2008. Diversity of deep-water cetaceans in relation to temperature: implications for ocean warming. Ecology Letters, 11(11): 1198-1207.
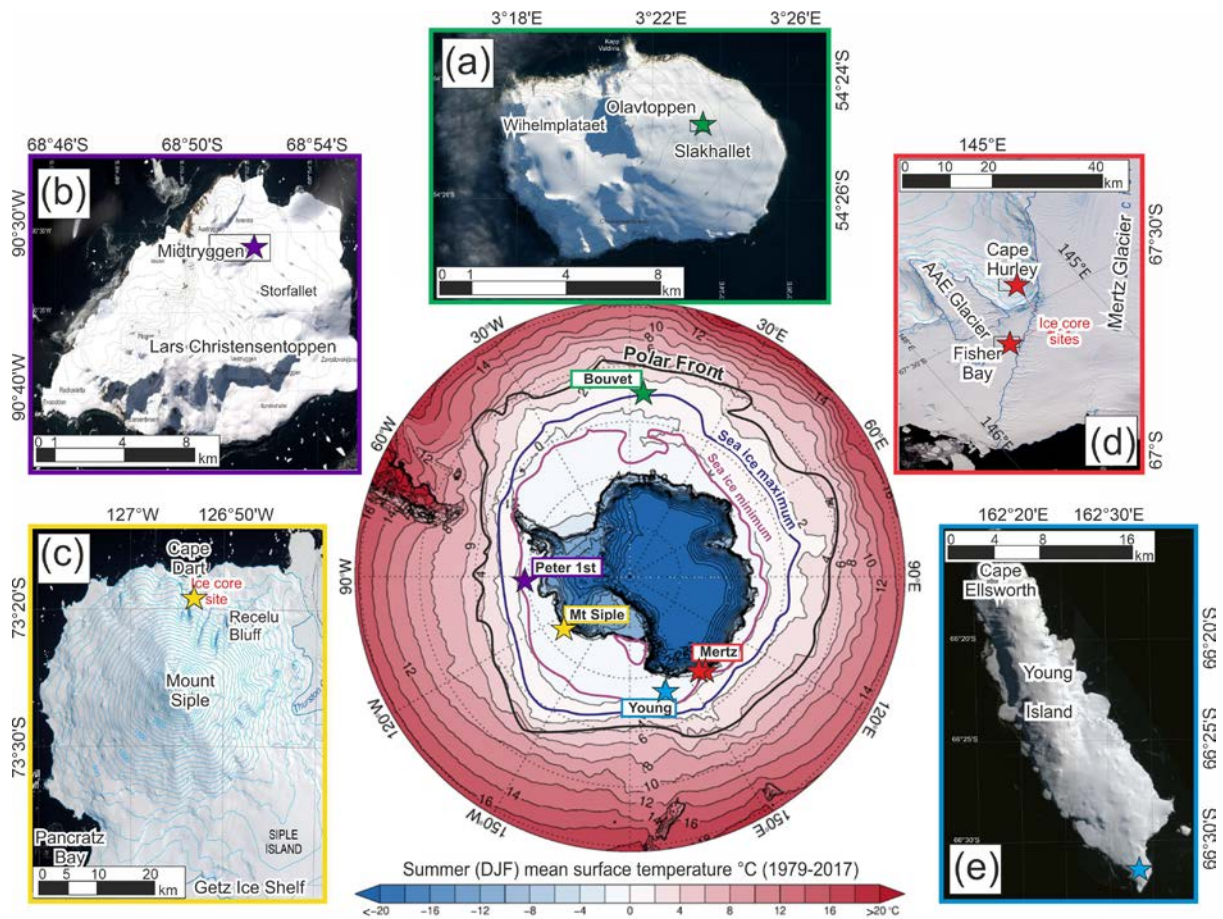
585

590

595

600

605

610

615

16

Figure 1: Map of subICE ice core locations (stars), with insert maps of each site. Overlain on mean summer surface temperatures (coloured contours) from ERA-5 (1979-2017). Location of the maximum (blue) and minimum (purple) sea ice extent, from NSIDC (1981-2017), and the Polar Front (black). (a) Bouvet Island, image credit Google Earth. (b) Peter 1st island and (c) Mount Siple, images from Sentinel-2 Copernicus data. (d) Map of Mertz glacier, showing the location of the two ice cores from Cape Hurley and Fisher Bay and (e) Young Island, Landsat image courtesy of USGS. All contours derived from TanDEM-X 90m DEM.
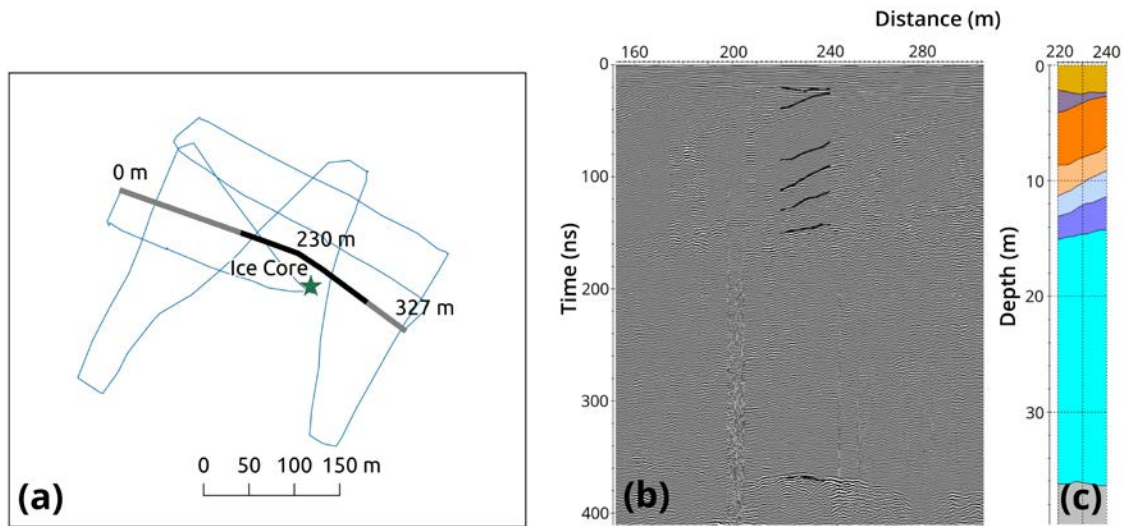
620

625

17

Figure 2: Bouvet GPR. (a) Reference map depicts the full track of measurements (blue), the profile (grey) and the section shown in the radargram (black). (b) Radargram obtained in a south easterly direction (downward) from 346 to 329 m a.s.l shown with layer interpretation and c) estimated depth of layers.
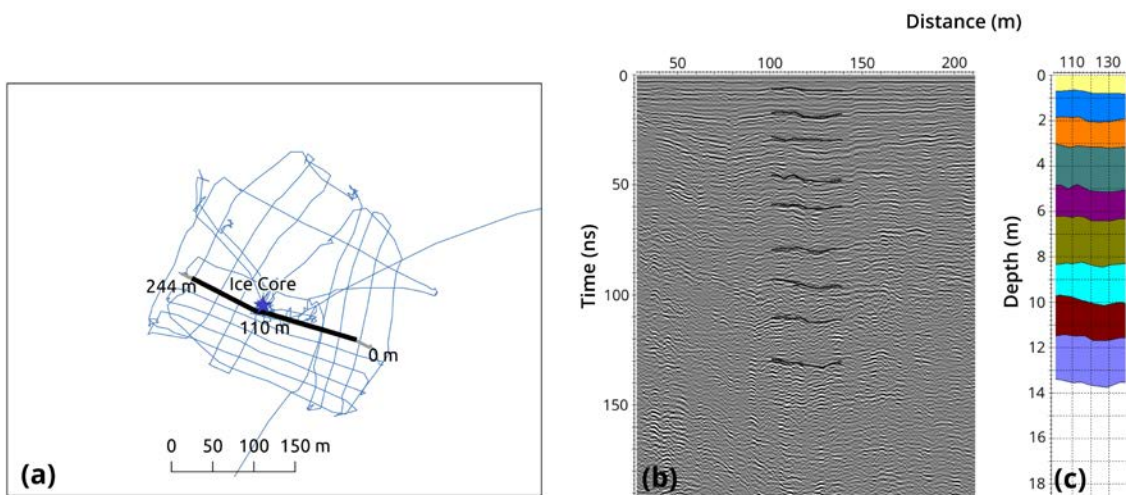

Figure 3: Peter 1st GPR. (a) Reference map depicts the full track of measurements (blue), the profile (grey) and the section shown in the radargram (black). (b) Section of a radargram taken in an east-westerly direction with layer interpretation and c) estimated depth of layers.
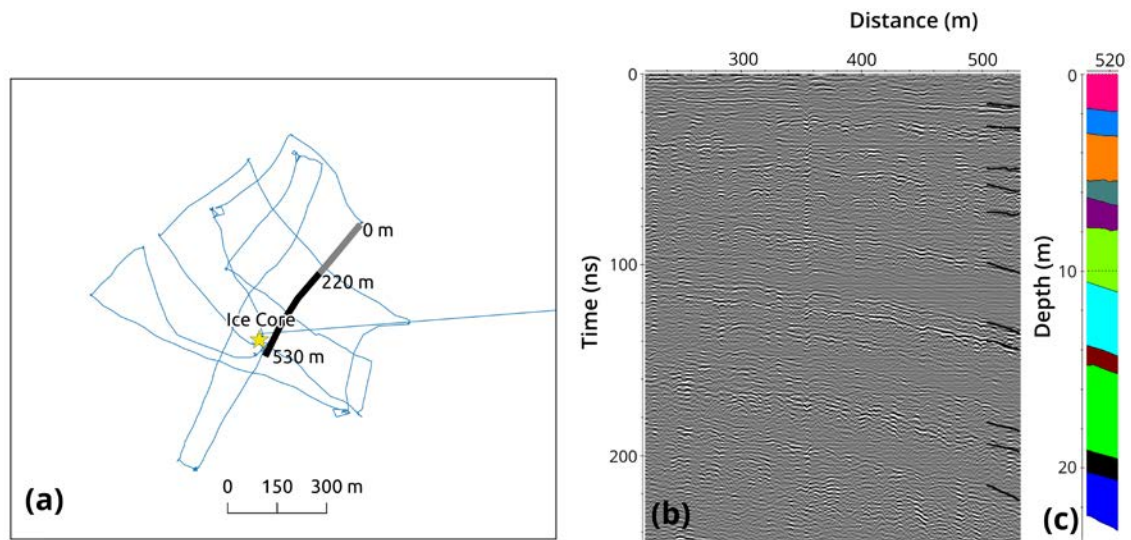
18

Figure 4: Mount Siple GPR. (a) Reference map depicts the full track of measurements (blue), the profile (grey) and the section shown in the radargram (black). (b) Radargram ending at the position of the ice core extraction (star) shown with layer interpretation and c) estimated depth of layers.
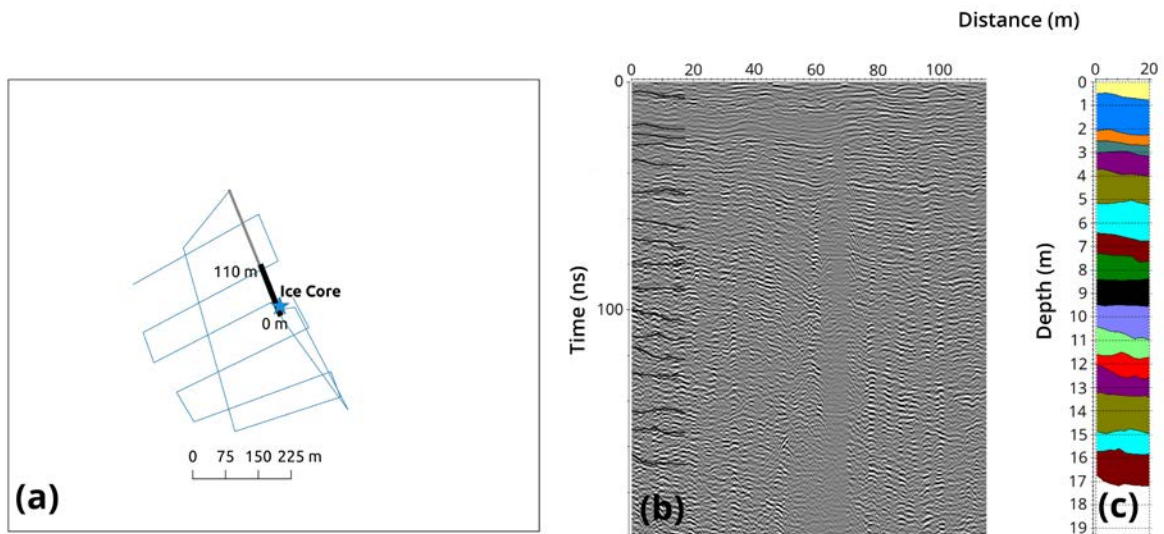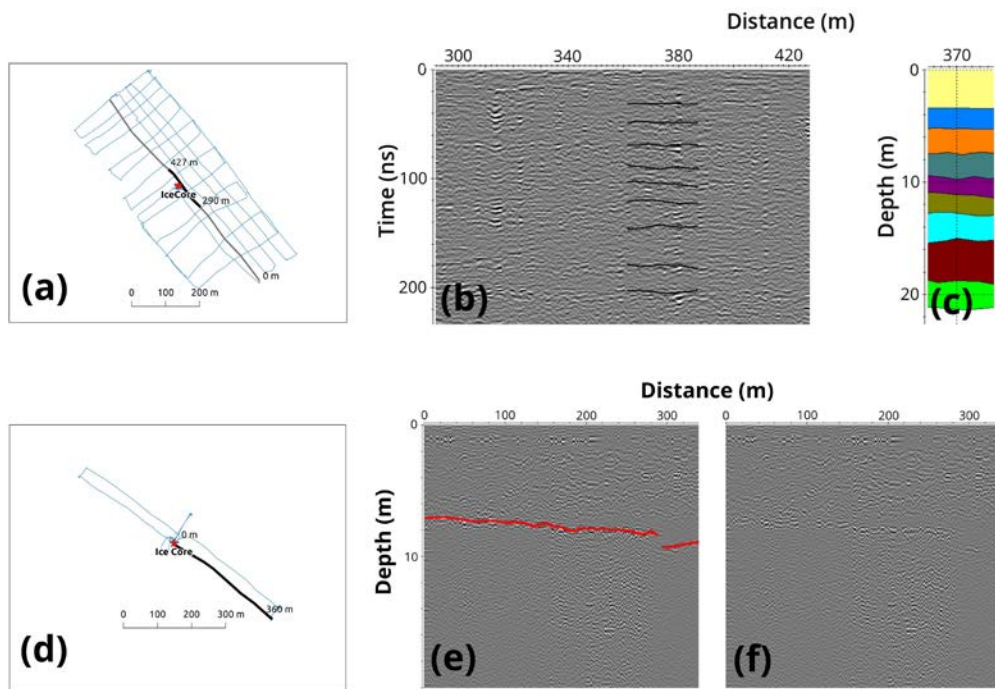

Figure 5: Young Island GPR. (a) Reference map depicts the full track of measurements (blue), the profile (grey) and the section shown in the radargram (black). (b) Section of a radargram obtained walking in direction NW from the ice core shown with layer interpretation and c) estimated depth of layers. A crevasse was detected at 70 m from the starting point (discontinuity in the reflections).

650

Figure 6: Mertz GPR. Reference maps of (a) Mertz 1 and (d) Mertz fast ice sites depicting the full track of measurements (blue), the profile (grey) and the section shown in the radargram (black). (b) Radargram representing a section of a transect crossing the ice core extraction point at Mertz 1 with layer interpretation and (c) estimated depth of layers. (e) Radargram collected at the 'fast ice' site, shown with one detected layer in red and (f) without
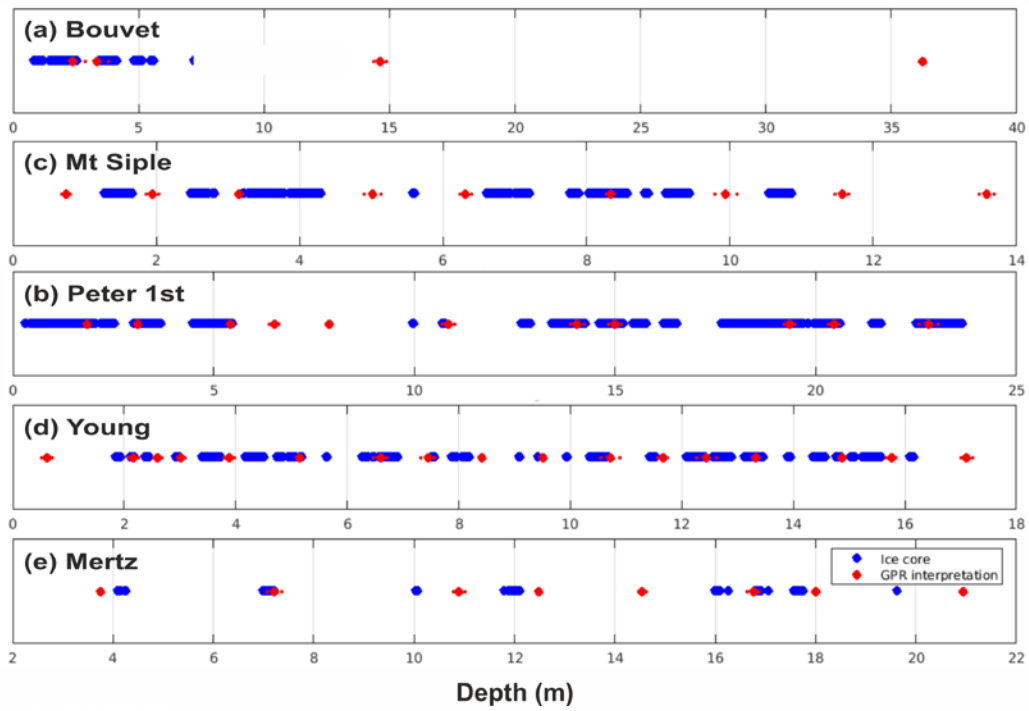
655 layer interpretation.

Figure 7: Comparison of detected layers (horizons) from GPR data (red dots, error bars 1 standard deviation) and the potentially visible patterns of melt derived from the reduced resolution ice core melt record (blue diamonds) for 660 each site.

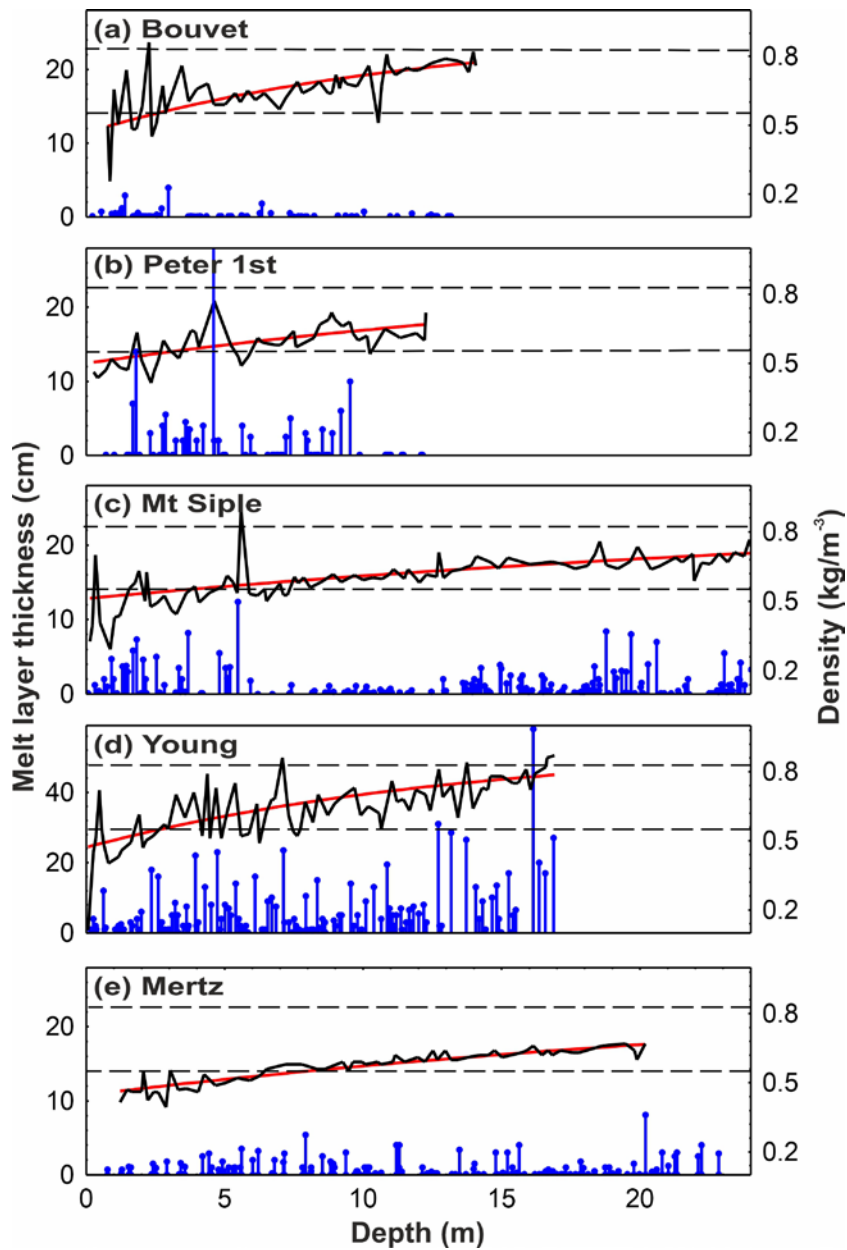**Figure 8: Melt layer thickness (blue/ cm), measured snow density (black) and fitted density curve (red) for each site**
(a) Bouvet, (b) Peter 1st island, (c) Mount Siple, (d) Young Island and (e) Mertz 1. Note the axis change for plot d
(Young Island). The horizontal lines represent the critical density (0.55 Kg m-3), and the pore close-off depth (0.83
Kg m-3).

670

675

22

Site name	Latitude	Longitude	Elevation (m)	ERA-5 annual average P-E	ERA-5 annual average (max) temperature (°C)		AWS max recorded temperature (°C) during years of operation.	
					2- m	Elevation corrected	AWS	Elevation corrected
Bouvet	54° 25' 19" S	03° 23' 27" E	350	0.72	-0.5 (2.3)	-2.9 (-0.1)	8.8 (1997-2005)	6.7
Peter 1st	68° 51' 05" S	90° 30' 35" W	730	0.56	-4.6 (1.3)	-9.5 (-3.7)	7.1 (2006)	3.0
Mt Siple	73° 19' 14" S	126° 39' 47" W	685	0.82	-9.6 (-0.3)	-14.2 (-5.0)	5.5 (1992-2015)	2.4
Young	66° 31' 44" S	162 33' 21"E	238	0.81	-7.6 (0.6)	-9.2 (-1.0)	4.2 (1991-1997)	2.8
Mertz	67° 33' 34" S	145° 18' 45"E	320	0.54	-15.2 (-1.1)	-17.4 (-6.3)	N/A	N/A
Mertz fast ice	67° 26' 28" S	145° 34' 28"E	6	0.66	-14.5 (-0.8)	N/A	N/A	N/A

685 **Table 1: Site meta-data for the subICE cores. Measured GPS location, elevation of ice core and ice core borehole depth. Annual average P-E, annual average temperature (maximum monthly temperature in brackets) from ERA-5 (1979-2017) at 2-m elevation and corrected for ice core elevation (using a lapse rate of 0.68 deg / 100 m). Where available the maximum recorded AWS temperature is shown, at the AWS elevation and corrected for ice core elevations, with years of operation in brackets.**

690

695

	GPR		Ice core		
Site name	Wave velocity (m/ns)	Max. depth detected (m)	Melt frequency (m^{-1}) and percentage	Average thickness (cm)	Maximum thickness (cm)
Bouvet	0.19	40	5.26 (1.6%)	0.3	4.0
Peter 1st	0.20	43	6.02 (11%)	1.8	30.0
Mt Siple	0.20	36	7.66 (10%)	1.3	12.4
Young	0.20	36	7.44 (47%)	6.4	58.0
Mertz 1	0.20	63	5.26 (6%)	1.0	8.1
Mertz fast ice	0.21	6.8	4.58 (0.3%)*	0.1	0.3

Table 2: Wave velocity and maximum depth detected from the GPR. Frequency (number of layers per meter), 710 percentage (% of whole core), average and maximum layer thickness measured in the ice cores. * Melt layers in the Mertz fast ice core were only measured in the top three bags (0-2.4 m).

	Ice core density		Age estimate	
Site name	Zero-depth intersection (m)	Close-off depth (m)	Ice core bottom age (AD)	Age at 100 m depth (AD)
Bouvet	0.5	28.7	2004 (+/- 3)	N/A
Peter 1st	0.5	34.5	2004 (+/- 2)	1856 (+/- 23)
Mt Siple	0.5	51.9	1998 (+/- 6)	1912 (+/- 35)
Young	0.5	21.1	2002 (+/- 4)	1874 (+/- 37)
Mertz 1	0.4	50.5	1994 (+/- 8)	1849 (+/- 64)
Mertz fast ice	0.0	7.2	2008 (+/- 3)	N/A

715 **Table 3: Ice core derived zero-depth intersection and close-off depth. Estimated age (years AD) at the bottom of the core and at 100 m, based on the measured ice core density.**

720